J_ID: CNE Customer A_ID: CNE24136 Cadmus Art: CNE24136 Ed. Ref. No.: 16-0193.R1 Date: 2-December-16 Stage: Page: 1

RESEARCH ARTICLE

Retinal Ganglion Cell Topography and Spatial Resolving Power in the White Rhinoceros (*Ceratotherium simum*)

João Paulo Coimbra* and Paul R. Manger

School of Anatomical Sciences, University of the Witwatersrand, Parktown 2193 Johannesburg, South Africa

ABSTRACT

This study sought to determine whether the retinal organization of the white rhinoceros (*Ceratotherium simum*), a large African herbivore with lips specialized for grazing in open savannahs, relates to its foraging ecology and habitat. Using stereology and retinal whole-mounts, we estimated a total of 353,000 retinal ganglion cells. Their density distribution reveals an unusual topographic organization of a temporal (2,000 cells/mm^2) and a nasal (1,800 cells/mm^2) area embedded within a well-defined horizontal visual streak (800 cells/mm^2), which is remarkably similar to the retinal organization in the black rhinoceros. Alpha ganglion cells comprise 3.5% (12,300) of the total population of ganglion cells and show a similar distribution pattern with maximum densities also occurring in the temporal (44 cells/mm^2) and nasal (40 cells/mm^2) areas. We found higher proportions of alpha cells in the dorsal and ventral retinas. Given their role in the detection of brisk transient stimuli, these higher proportions may facilitate the detection of approaching objects from the front and behind while grazing with the head at 45°. Using ganglion cell peak density and eye size (29 mm, axial length), we estimated upper limits of spatial resolving power of 7 cycles/deg (temporal area), 6.6 cycles/deg (nasal area), and 4.4 cycles/deg (horizontal streak). The resolution of the temporal area potentially assists with grazing, while the resolution of the streak may be used for panoramic surveillance of the horizon. The nasal area may assist with detection of approaching objects from behind, potentially representing an adaptation compensating for limited neck and head mobility. J. Comp. Neurol. 000:000–000, 2016.

INDEXING TERMS: retinal topography; perissodactyls; retinal ganglion cells; alpha ganglion cells; stereology; spatial resolving power; RRID: AB_477257; RRID: SciRes_000114; RRID: SciRes_000116

Rhinoceroses comprise a small, but diverse, group of the odd-toed hoofed mammals (Perissodactyla) (Price and Bininda-Emonds, 2009; Dinerstein, 2011). They occupy a wide variety of habitats with distinct structural complexities ranging from open grasslands and woodlands in Africa to enclosed rainforests and floodplains with tall grass in Asia (Dinerstein, 2011). All species of rhinoceroses are herbivores and can be predominantly grazers or browsers, or may alternate between these two feeding methods depending on the seasonal availability of plant material (Dinerstein, 2011). They exhibit important morphological adaptations of their oral labia that allow them to exploit a diverse range of vegetation types and occupy distinct feeding niches (Dinerstein, 2011). For example, the black rhinoceros (*Diceros bicornis*) is a browser with a prehensile upper lip that facilitates plucking leaves and grasping stems in relatively more enclosed woodland microhabitats (Hillman-Smith and Groves, 1994). In contrast, the white rhinoceros (*Ceratotherium simum*) is a strict grazer having specialized broad and square lips that enable the clipping of the grass close to the ground in open savannah habitats (Groves, 1972).

Variations in the topographic distribution of retinal neurons generally reflect ecological variables (i.e., feeding niche and habitat type) and are key predictors of the relative importance of vision to behavior (Hughes,

Grant sponsor: the National Research Foundation of South Africa (to P.R.M.); Grant number: 96263; Grant sponsor: URC postdoctoral fellowship at The University of the Witwatersrand (to J.P.C.).

*CORRESPONDENCE TO: João Paulo Coimbra, School of Anatomical Sciences, The University of the Witwatersrand, Parktown 2193, Johannesburg, South Africa. E-mail: jp.coimbra13@gmail.com

Received September 16, 2016; Revised October 13, 2016;
Accepted October 25, 2016.
DOI 10.1002/cne.24136
Published online Month 00, 2016 in Wiley Online Library (wileyonlinelibrary.com)

ID: jwaa3b2server Time: 21:15 I Path: //chenas03/Cenpro/ApplicationFiles/Journals/Wiley/CNE#/Vol00000/160154/Comp/APPFile/JW-CNE#160154

1977; Collin, 1999). Elongated topographic patterns (i.e., horizontal streaks) of retinal neuronal density distributions, which are common in species that occur in more open microhabitats, allow for improved panoramic visual sampling across the horizon (Hughes, 1977; Collin, 1999). In contrast, concentric patterns (i.e., areas), which are found in species that occur in more enclosed microhabitats, allow for enhanced visual sampling in a more localized portion of the visual field (Hughes, 1977; Collin, 1999). In the black rhinoceros, the only species of rhinoceros examined to date, the topographic distribution of retinal ganglion cells reveals a remarkably unusual organization for terrestrial mammals. In this species, retinal ganglion cells reach their maximum density in two concentric areas located in the temporal and nasal portions of the retina, which enables simultaneous vision in the frontal and posterior visual fields, presumably assisting with foraging and predator detection, respectively (Pettigrew and Manger, 2008). The level of spatial resolution afforded by these two areas (~5–6 cycles/deg) is sufficient to allow the black rhinoceros to detect small leaves at relevant foraging distances. Moreover, black rhinoceroses also have a horizontal streak of high density of retinal ganglion cells, which allows for enhanced panoramic vision across the horizon, and potentially facilitates the detection of predators and conspecifics (Pettigrew and Manger, 2008).

Despite the wealth of information that can be predicted about habitat use and foraging ecology from retinal organization (Hughes, 1977; Collin, 1999), no information is available about the topographic distribution of neurons in the retina of the white rhinoceros. Here we sought to determine whether the retina of the white rhinoceros shows a dual topographic organization similar to that of the black rhinoceros or whether it shows variations that reflect their grazing habits (i.e., lower visual resolution) and occurrence in open environments (i.e., more pronounced horizontal streak). Using retinal wholemounts and stereology, we mapped the topographic distribution of the total population of retinal ganglion cells and estimated the upper limits of spatial resolution of the white rhinoceros eye. We also mapped the population of presumed alpha retinal ganglion cells in Nissl-stained wholemounts and confirmed our cytological criteria with neurofilament immunohistochemistry. In mammals, alpha cells comprise a morphologically distinct type of retinal ganglion cells, which are rich in neurofilaments and have large cell bodies and dendritic trees (Peichl et al., 1987; Peichl, 1991; Sanes and Masland, 2015). Alpha cells are presumably involved with the detection of brisk transient stimuli (Peichl et al., 1987; Peichl, 1991) and approaching or receding objects (Sanes and Masland, 2015), which may be ecologically relevant for the detection of predators and conspecifics.

MATERIALS AND METHODS

Specimen

One 3-year-old female white rhinoceros was used in the present study. This female rhinoceros survived a poaching attempt; however, a bullet severed the right radial nerve, preventing rehabilitation. The animal was humanely euthanized for veterinary reasons, and the eyes were made available for the present investigation. The harvesting of tissue from this specimen was approved by the University of the Witwatersrand Animal Ethics Committee (clearance number 2008/36/1). Because other studies in many vertebrates have shown that interindividual variation in the total number and topographic distribution of retinal ganglion cells is generally low (Coimbra et al., 2013, 2014a, 2014b; Lisney et al. 2012, 2013a, 2013b; de Busserolles et al., 2014), and given the endangered status of the white rhinoceros, the eyes from this single specimen were considered representative for the characterization of the retinal topographic specializations in this species.

Perfusion and retinal wholemount preparation

After euthanasia, the head of the white rhinoceros was removed and perfused following the method described in Manger et al. (2009). In brief, both carotid arteries were located and a cannula (6-mm outer diameter, 4-mm inner diameter) was inserted and secured in place. Subsequently, approximately 5 liters of 0.9% saline followed by 5 liters of 4% paraformaldehyde in 0.1 M phosphate buffer (PB), pH 7.2–7.4 were flushed through the head via carotid arteries. The eyes were oriented with a cauterization mark on the dorsal portion of the cornea (Coimbra et al., 2013), removed from the head, immersed in fixative for a further 24 hours, and subsequently stored in 0.1 M PB (pH 7.2–7.4) containing 0.1% sodium azide.

Retinal wholemounts were prepared and processed following standard methods (Stone, 1981; Coimbra et al., 2006). Briefly, the cornea and vitreous were removed, and the retinas were dissected by making radial cuts from the periphery to the center of the eyecup. Remnants of the retinal pigment epithelium attached to the retinal wholemounts were bleached with 3% hydrogen peroxide in 0.1 M PB for approximately 12 hours at room temperature (Coimbra et al., 2009).

ID: jwaa3b2server Time: 21:15 I Path: //chenas03/Cenpro/ApplicationFiles/Journals/Wiley/CNE#/Vol00000/160154/Comp/APPFile/JW-CNE#160154

Nissl staining

To estimate the total number and map the topographic distribution of ganglion cells (total and alpha), one retinal wholemount (right) was mounted vitreous side up onto a gelatinized slide for staining with the Nissl method (Stone, 1981; Coimbra et al., 2006). To improve the adherence of the retinal wholemount to the slide and enhance staining, the retinal wholemount was incubated in formaldehyde vapors at room temperature overnight (Stone, 1981). The retinal wholemount was then rehydrated, stained for 5 minutes with an aqueous solution of 0.1% cresyl violet (Sigma), dehydrated in an ethanol series, cleared in xylene, and finally coverslipped with Entellan New (Merck, Modderfontein, South Africa) (Coimbra et al., 2006). As the retinal wholemount was attached to the slide during all staining steps, shrinkage was considered to be negligible and confined to the borders of the ora serrata and the edges of the radial cuts (Wässle et al., 1975; Peichl, 1992).

Immunohistochemistry

To validate our cytological criteria to identify alpha ganglion cells, the other retinal wholemount (left) was used for neurofilament immunohistochemistry. Antibodies against the heavy subunit of neurofilaments label a population of large ganglion cells in the retinas of a variety of mammals including marsupials (big-eared opossum; Moraes et al., 2000), rodents (mouse; Dräger and Hofbauer, 1984), primates (human; Straznicky et al., 1992; Ruiz-Ederra et al., 2004), and artiodactyls (pig; Ruiz-Ederra et al., 2004; giraffe, Coimbra et al., 2013).

For the immunohistochemistry procedures described below, we performed all incubations at room temperature and used 0.1 M PB (pH 7.2–7.4) for rinsing and preparing all incubating solutions. To improve antibody permeability, the retinal wholemount was treated with 0.1% collagenase for 10 minutes and then rinsed for 5 minutes. To further permeabilize and inhibit endogenous peroxidases, the retinal wholemount was then incubated in a solution containing 10% methanol and 3% hydrogen peroxide for 40 minutes. Subsequently, to both rinse and further permeabilize, the retinal wholemount was treated with 5% Triton X-100 (Sigma, St. Louis, MO) for 5 minutes (twice) and then for a further 20 minutes. Subsequently, the wholemount was rinsed three times for 5 minutes each and then incubated in a mixture containing the anti-neurofilament 200 primary antibody (1:3,000; clone N52, N0142, Sigma), 5% normal donkey serum (Millipore, Billerica, MA), and 1% Triton X-100 for 24 hours with gentle rocking. The retinal wholemount was rinsed three times for 5 minutes each and incubated in biotinylated donkey anti-mouse secondary antibody (1:500, Jackson ImmunoResearch, West Grove, PA) for 2 hours. The retinal wholemount was then transferred to a solution containing avidin–biotin complex (Vectastain ABC kit, Vector, Burlingame, CA) and further incubated for 1 hour. Finally, the retinal wholemount was rinsed three times for 5 minutes each before reaction in a solution containing SG as the chromogen (Peroxidase Substrate kit, Vector). After the reaction, the retinal wholemount was rinsed overnight, mounted vitreal side up onto a large gelatinized slide, and allowed to dry overnight at room temperature. Subsequently, the retinal wholemount was rehydrated, then dehydrated in an ascending ethanol series, cleared with xylene, and mounted with Entellan New (Coimbra et al., 2013). As the retinal wholemount was attached to the slide during the dehydration stages, shrinkage was considered to be negligible.

Antibody characterization and specificity

Monoclonal anti-neurofilament 200 antibodies are raised against the C-terminal of pig neurofilament H-subunit polypeptides. This antibody clone is reported to recognize both phosphorylated and nonphosphorylated forms of neurofilaments with 200 kDa molecular weight as detected in immunoblotting (Sigma-Aldrich, St. Louis, MO, clone N52, Cat# N0142, RRID: AB_477257). This antibody does not cross-react with other intermediate filaments, and its specificity in the nervous system has been tested elsewhere using western blots from rat spinal cord homogenates (Hubert et al., 2008; Yamanaka et al. 2011). The immunostaining pattern observed using anti-neurofilament 200 (clone N52) reveals intense labeling of neurofibrils in the soma, dendrites, and axons of neurons. The neurofilament-200 (clone N52) immunostaining pattern obtained in this study is consistent with labeling shown in previous reports in the mammalian retina using the antibody from the same manufacturer (Moraes et al., 2000; Coimbra et al., 2013). Secondary antibody specificity was assessed by incubating small retinal pieces in a mixture in which the primary antibody had been omitted (Saper and Sawchenko, 2003). No labeling was detected.

Estimation of the total number and topographic distribution of retinal ganglion cells using stereology

Using the optical fractionator method (West et al., 1991) with modifications for the use in retinal wholemounts (Coimbra et al., 2009, 2012), we estimated the total number and the topographic distribution of retinal

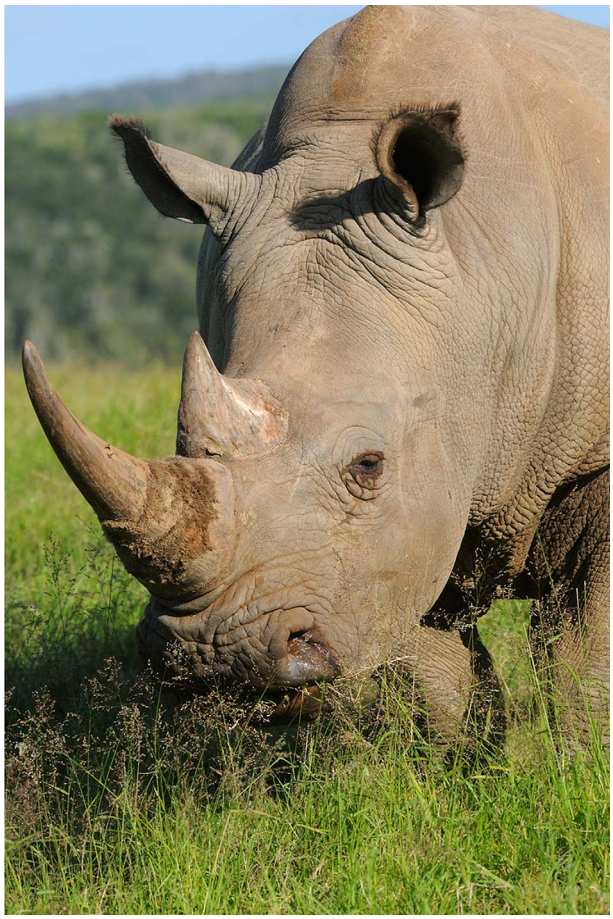

Figure 1. Close-up of the head of the white rhinoceros during grazing. Photo credit: Malcolm Schuyl. [Color figure can be viewed at wileyonlinelibrary.com]

ganglion cells in the white rhinoceros. Briefly, the retina was considered as one single section and therefore the section sampling fraction (ssf) was 1. As the retinal ganglion cell layer in the white rhinoceros comprises a single layer of neurons, the optical disector height was the same as the thickness of the ganglion cell layer at all eccentricities to give a thickness sampling factor (tsf) of 1. Therefore, only the area sampling fraction (asf), which is the ratio between the counting frame and the sampling grid, was used to estimate the total number of retinal ganglion cells according to the following algorithm:

$$N\text{total} = \Sigma Q \times 1/\text{asf}$$

where ΣQ is the sum of total neurons counted (West et al., 1991).

The outlines of the white rhinoceros retinal wholemounts were digitized using a $4\times$/NA 0.13 objective on a microscope (Olympus BX50) equipped with a motorized stage (MAC200; Ludl Electronics Products, Hawthorne, NY) and connected to a computer running Stereo Investigator software (http://www.mbfbioscience.com, RRID: SciRes_000114). The ganglion cell layer was outlined close to the limits of the retinal borders (at the ora serrata) and along the radial cuts, but excluding other retinal layers that can be seen in transverse view after wholemounting. The outline of the base of the optic disc was subtracted from the total ganglion cell layer area.

Under microscopic examination, we noticed that retinal ganglion cell density increased in the equator of the retina forming a band of high density (Fig. 2A). Demarcation of this band allowed us to use different sampling strategies to optimize counting and detect variations in density (Fig. 2B, Table 1). Within each demarcated region, sampling grids were placed in a random, uniform, and systematic fashion. At each sampling site, we counted only retinal ganglion cells (total and alpha) that lay entirely within the counting frame, or that intersected the acceptance lines without touching the rejection lines (Gundersen, 1977). Upon identification of the highest density region within the high-density band, we used a high-frequency sampling scheme around the two highest density values to confirm the magnitude and location of the peak density of total retinal ganglion cells (Table 1). Because the counting frames used to estimate alpha ganglion cell density covered a larger proportion of the sampling grid size, subsampling was not needed to confirm estimates of peak density. These stereological parameters were chosen on the basis of pilot experiments to achieve a Schaeffer coefficient of error (CE) < 0.1, which is deemed appropriate in the present study because variances introduced by the counting procedures contribute very little to the observed group variance (Glaser and Wilson, 1998; Slomianka and West, 2005).

To distinguish retinal ganglion cells from amacrine and glial cells in the white rhinoceros Nissl-stained wholemount, we used well-established cytological criteria proposed by Hughes (1981a). These criteria have been validated in a range of mammals including perissodactyls (Wong et al., 1986; Silveira et al., 1989a,b; Peichl, 1992; Mass and Supin, 1992; Harman et al., 1999; Pettigrew and Manger, 2008; Coimbra et al., 2013, 2015, 2016, 2017). Cell profiles showing polygonal soma with dense accumulations of Nissl substance in the cytoplasm, an eccentric nucleus, and a prominent nucleolus were classified as retinal ganglion cells (Fig. 2C,D). Smaller, rounder, and more palely stained profiles, with no evident Nissl substance in the cytoplasm, were classified as amacrine cells (Fig. 2C,D). Darkly stained profiles displaying a small, round, or slightly elongated cell body were recognized as glial cells (Fig. 2C,D). The white rhinoceros retina is

ID: jwaa3b2server Time: 21:15 I Path: //chenas03/Cenpro/ApplicationFiles/Journals/Wiley/CNE#/Vol00000/160154/Comp/APPFile/JW-CNE#160154

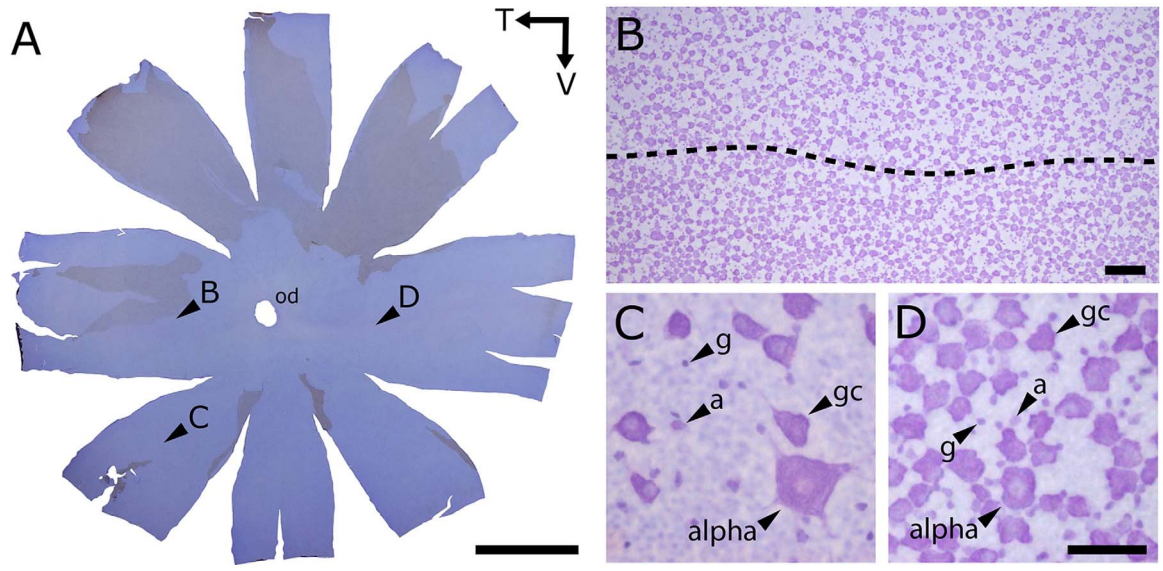

Figure 2. Nissl-stained retinal wholemount of the white rhinoceros (**A**). Note the homogeneous staining across the preparation except for slightly darker region in the retinal equator (A). Under microscopic inspection, the limits of the band of high neuronal density were demarcated as depicted by the dashed line (**B**). Cytological criteria used to distinguish retinal ganglion cells (gc) from amacrine (a) and glial (g) in low (**C**) and high (**D**) density regions are indicated in A. Criteria to identify alpha ganglion cells (alpha) are also shown (C, D). od, optic disc; T, temporal; V, ventral. Scale bars = 10 mm in A; 50 μm in B; 100 μm in D (also applies to C). [Color figure can be viewed at wileyonlinelibrary.com]

TABLE 1.

Stereological Parameters Defined to Estimate the Total Number and Topographic Distribution of Total and Alpha Retinal Ganglion Cells in the White Rhinoceros Nissl-Stained Retinal Wholemount Using the Optical Fractionator Method

Neuron type/ sampling region	Counting frame (μm)	Grid (μm)	Area sampling fraction	Objective/numerical aperture
Total ganglion cells				
Periphery	350 × 350	2,800 × 2,800	0.0156	40×/0.6 air
Streak	170 × 170	600 × 600	0.0803	40×/0.6 air
Subsampling	150 × 150	250 × 250	0.3600	40×/0.6 air
Alpha ganglion cells				
Periphery	1,000 × 1,000	4,000 × 4,000	0.0625	10×/0.3 air
Streak	500 × 500	950 × 950	0.2770	10×/0.3 air

avascular, and hence no endothelial cells were identified (Johnson, 1901). These cytological criteria were consistent at all eccentricities and were unambiguously applicable in regions of low and high density (Fig. 2C,D). Because retinal ganglion cells were reliably identified at all eccentricities, we opted to exclude other cell types from the counting procedures. Moreover, we were also able to distinguish presumed alpha ganglion cells from non-alpha cells based on their cytological features. These cells showed very large polygonal soma and dense accumulations of Nissl substance (Fig. 2C,D) resembling the alpha cells found in cats and other mammals (Wässle et al., 1975; Peichl et al., 1987; Peichl, 1991).

To obtain a systematic random sampling of the soma sizes of alpha cells across the retina, we used the nucleator probe within an optical fractionator sampling scheme (Gundersen et al., 1988). Because of the low density of alpha cells in both Nissl- and neurofilament-stained retinal wholemounts, we used a large counting frame of 500 × 500 μm. Within the band of high density, we sampled three regions (temporal, central, and nasal) using a grid size of 950 × 950 μm. Outside the band, we sampled four regions (dorsal, ventral, temporal, and nasal) in the retinal midperiphery using a grid size of 1,500 × 1,500 μm. These regions were selected approximately at 15 mm (temporal) and 20 mm (other retinal regions) from the optic disc. Within each counting frame, we marked alpha ganglion cell profiles using the nucleolus as reference. To estimate the soma area, we marked the intersections of six rays emanating from the nucleolus with the boundaries of the alpha cell soma. For convenience, soma areas were converted into soma diameters. We used the same counting rules

TABLE 2.

Estimates of the Total Number (rounded to the nearest 1,000) and Peak Density of Total (rounded to the nearest 100) and Alpha Ganglion Cells Obtained From the Nissl-Stained Retinal Wholemount of the White Rhinoceros Using the Optical Fractionator Method

Neuron type/ sampling region	Retinal area (mm^2)	Number of sites counted	Estimated total number	CE	Peak density (cells/mm^2)
Total ganglion cells					
Periphery	1,587	214	284,000	0.055	
Streak	63	205	69,000	0.035	
Total	1,650	419	353,000		
Mean				0.045	
Subsampling					
Temporal area	1.44	20		0.071	2,000
Nasal area	1.13	18		0.067	1,800
Alpha ganglion cells					
Periphery	1,587	114	10,900	0.065	
Streak	63	101	1,400	0.061	
Total	1,650	215	12,300		
Mean				0.063	
Temporal area					44
Nasal area					40

as described above for our optical fractionator estimates (Gundersen, 1977). Nucleator CE was < 0.008 for all samples.

Topographic maps illustrating variations of retinal ganglion cell density were constructed using Arcview 3.2 software (http://www.esri.com, RRID: SciRes_000116) using the spline interpolation method (Coimbra et al., 2006). Photomicrographs were obtained using a digital camera (Microfire, Optronics, Fremont, CA) coupled to a Stereo Investigator system. Digital photomicrographs were processed using Adobe Photoshop CS2 (San Jose, CA) for scaling and minor adjustment of the levels of brightness and contrast.

Anatomical estimation of spatial resolving power

Anatomical estimates of spatial resolving power were obtained for the eye of the white rhinoceros. We obtained an estimate of the posterior nodal distance (PND) of the eye by multiplying the eye axial length by 0.57, which is the ratio between PND and axial length described for cathemeral species (Pettigrew et al., 1988). White rhinoceroses show peak activity early in the morning (5–9 am) and later in the afternoon (3–6:30 pm) (Groves, 1972).

To estimate the retinal magnification factor (RMF), which represents the distance in retinal surface that subtends 1 degree, we used the equation (Pettigrew et al., 1988):

$$RMF = 2\pi PND/360$$

We assumed that retinal ganglion cells in the high-density regions occur in a triangular lattice because this arrangement allows for the minimum center-to-center spacing among cells (Williams and Coletta, 1987). To estimate the Nyquist limits of spatial resolution, we used the retinal ganglion cell peak density (D) according to the equation (Snyder and Miller, 1977; Williams and Coletta, 1987):

$$f_N = 0.5 \times RMF \times (2D/\sqrt{3})^{1/2}$$

Anatomical estimates of spatial resolving power using the total peak density of retinal ganglion cells represent upper limits of retinal resolution because it is unknown, for this species, what percentage of retinal ganglion cells is involved in resolution tasks (Wässle, 2004; Reuter and Peichl, 2008).

To relate behavioral significance to our estimates of spatial resolving power, we predicted the minimum object size (i.e., grass, predator) that a white rhinoceros could spatially resolve given optimal conditions of contrast and luminance. First, by calculating the inverse of the spatial resolving power, we estimated the angular distance in the retina that corresponds to one cycle. Then this value was divided by 2 to obtain the minimum angle of resolution (MAR), which is equivalent to half a cycle (i.e., one black bar) and represents the angular distance of the smallest resolvable detail on the retina. Subsequently, using the trigonometric relationships between the minimum angle of resolution and a presumed distance relevant for foraging and predator detection (D), we estimated the minimum object size (Obj) using the equation:

$$D = Obj/\tan MAR$$

According to the Nyquist sampling theorem (Hughes, 1981b), an object needs to be twice the threshold to

ID: jwaa3b2server Time: 21:15 I Path: //chenas03/Cenpro/ApplicationFiles/Journals/Wiley/CNE#/Vol00000/160154/Comp/APPFile/JW-CNE#160154

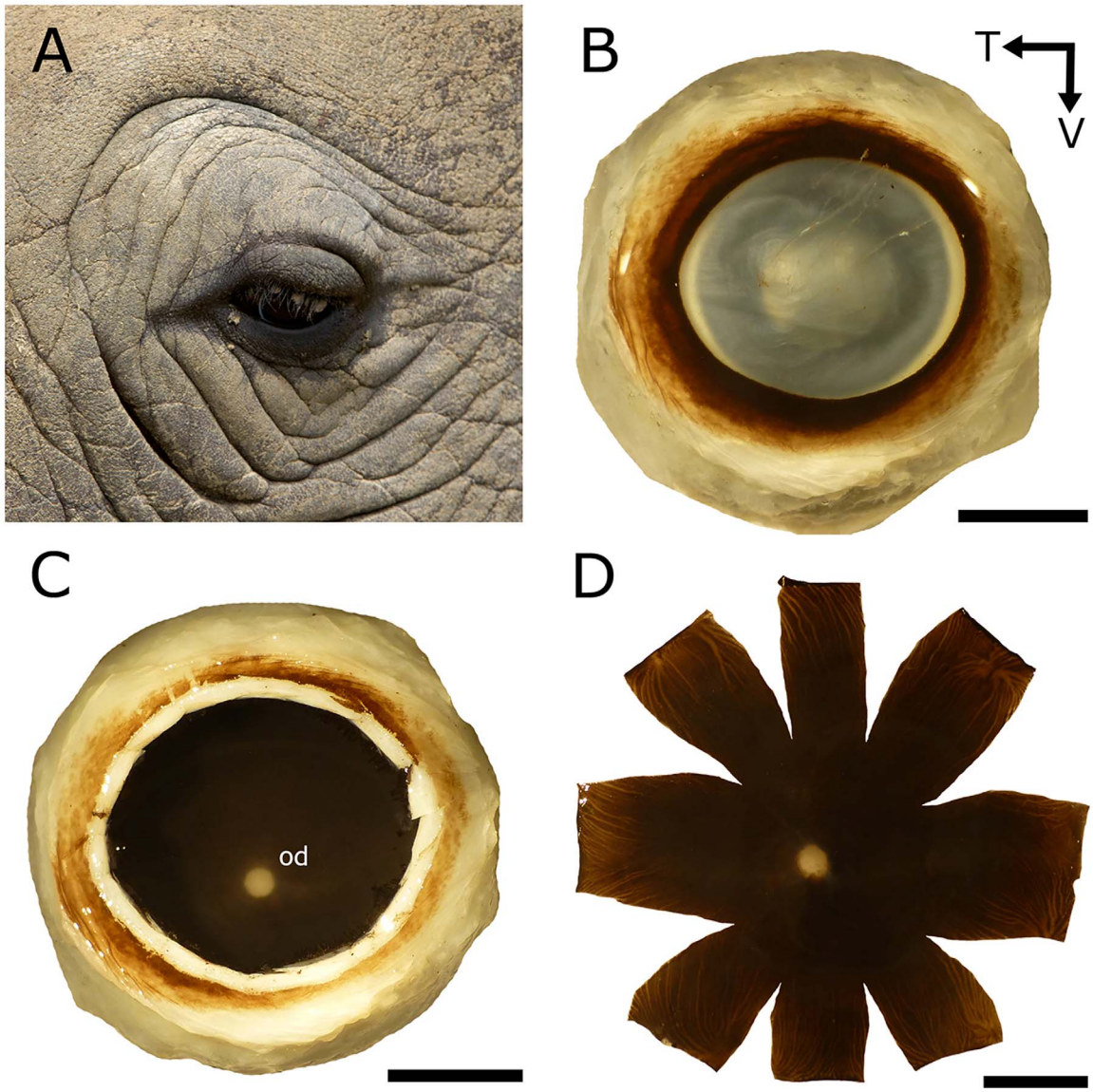

COLOR ONLINE AND BW IN PRINT

Figure 3. Close-up of the right eye in the head (**A**), whole eye (**B**), eyecup (**C**), and flattened choroid (**C**) of the white rhinoceros. Note that the eye is relatively spherical. Note that the eye fundus as shown by the eyecup (C) and flattened choroid (D) shows homogeneous brown coloration with no indication of a tapetum lucidum. Photo credit: Malcolm Schuyl (A). od, optic disc; T, temporal; V, ventral. Scale bars = 10 mm in B–D. [Color figure can be viewed at wileyonlinelibrary.com]

be spatially resolved. Hence the minimum object size estimated was multiplied by 2.

RESULTS

The eye of the white rhinoceros

F3 The eye of the white rhinoceros (Fig. 3A) is spherical, with a mean nasotemporal diameter of 32.2 mm (32.1 mm, left; 32.2 mm right) and dorsoventral diameter of 31.9 (31.8 mm, left; 32 mm right) (Fig. 3B). Mean eye axial length was 29.3 mm (28.9 mm, left; 29.6 mm right). The eye fundus was dark throughout its extension with no indication of a tapetum lucidum (Fig. 3C), as confirmed by the wholemounted choroid (Fig. 3D).

Number and topographic distribution of retinal ganglion cells

In the Nissl-stained retinal wholemount of the white rhinoceros, we estimated a total of ~ 353,000 retinal ganglion cells. Topographic mapping of total retinal ganglion cell densities revealed a horizontal streak running through and below the optic disc as demarcated by an isodensity line of 200 cells/mm^2 (Fig. 4A). Within the F4 temporal and nasal poles of the horizontal streak, isodensity lines of 1,000 cells/mm^2 were more concentrically organized and delineated a temporal and a nasal area of high ganglion cell density (Fig. 4A). Retinal ganglion cells reached maximum density of ~2,000 cells/

ID: jwaa3b2server Time: 21:15 I Path: //chenas03/Cenpro/ApplicationFiles/Journals/Wiley/CNE#/Vol00000/160154/Comp/APPFile/JW-CNE#160154

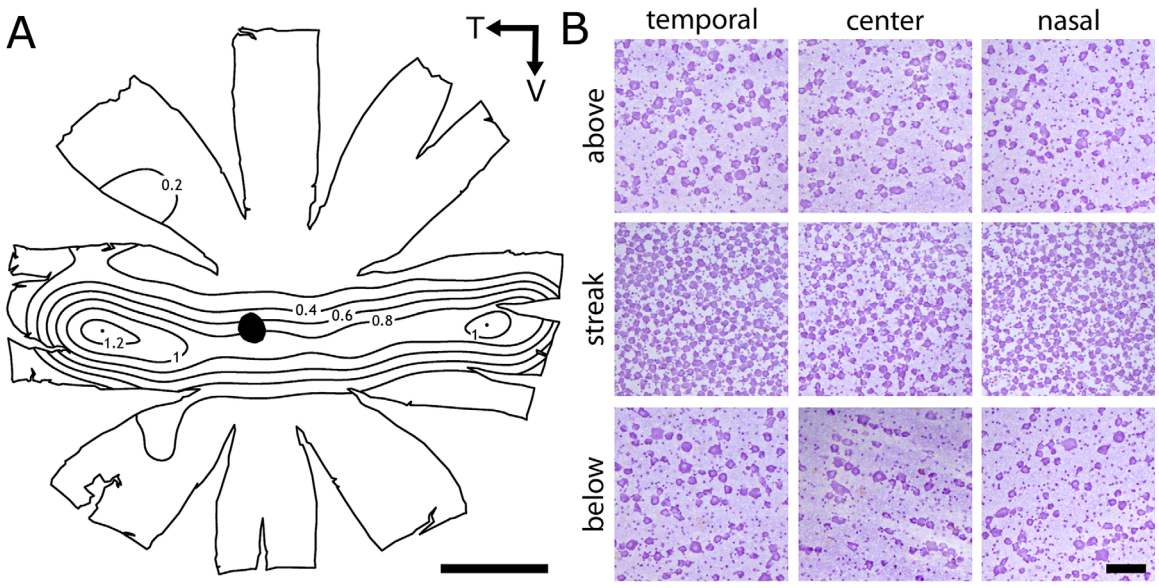

COLOR ONLINE AND BW IN PRINT

Figure 4. Topographic map illustrating the distribution of retinal ganglion cell densities in the Nissl-stained retinal wholemount of the white rhinoceros (**A**). Note the presence of a temporal and a nasal area embedded in well-defined horizontal streak demarcated by an isodensity line of 200 cells/mm^2. Isodensity lines of 1,000 cells/mm^2 delineating the temporal and nasal areas were more concentric. The dots within the limits of the isodensity lines of 1,200 cells/mm^2 and 1,000 cells/mm^2 mark the location of the peak density of retinal ganglion cells in the temporal (~2,000 cells/mm^2) and nasal (~1,800 cells/mm^2) areas, respectively. Changes in density gradients are clearly seen in photomicrographs taken in vertical transects through the temporal, central, and nasal portions of the horizontal streak (**B**). The black circle in A indicates the position of the optic disc. Numbers on the isodensity lines should be multiplied by 10^3 to express densities in cells/mm^2. T, temporal; V, ventral. Scale bars = 10 mm in A; 100 μm in B (applies to all photomicrographs in B). [Color figure can be viewed at wileyonlinelibrary.com]

mm^2 in the temporal area, and ~1,800 cells/mm^2 in the nasal area. In the periphery and midperiphery, retinal ganglion cell density varied between 50 and 100 cells/mm^2. Variations in retinal ganglion cell density can be clearly detected in transects through the temporal, central, and nasal portions of the visual streak in the Nissl-stained wholemount (Fig. 4B).

Using cytological criteria, we mapped the population of presumed alpha cells in the retina of the white rhinoceros. We estimated a total of ~12,300 alpha cells comprising ~3.5% of the total ganglion cell population. Topographic mapping of alpha cells revealed a broad peripheral plateau delineated by an isodensity line of 5 cells/mm^2 (Fig. 5A). This plateau is asymmetric, occupying a larger area in the dorsal compared with the ventral retina (Fig. 5A). Toward the equator of the retina, an isodensity line of 10 cells/mm^2 demarcated a horizontal streak (Fig. 5A). Within the temporal and nasal portions of this streak, alpha cells form two high-density areas demarcated by isodensity lines of 15 cells/mm^2 (Fig. 5A). Alpha ganglion cells reached a maximum density of ~44 cells/mm^2 in the temporal area, and ~40 cells/mm^2 in the nasal area. Alpha ganglion cell profiles identified in the Nissl-stained retina showed large soma size with stellate morphology similar to alpha cells stained by neurofilaments in regions of high (Fig. 5B–E) and low (Fig. 5F–I) density.

Alpha ganglion cell proportion and size varied across retinal regions in the white rhinoceros. We found good correspondence between estimates of the proportions and soma sizes of alpha ganglion cells across different regions in Nissl- and neurofilament-stained retinas of the white rhinoceros (Fig. 6). The proportions of alpha cells are slightly higher (~7.5%, Nissl and neurofilament) in the dorsal retina compared with the ventral retina (~6.5%, Nissl; 5.5%, neurofilament). Alpha cells occur in their lowest proportions in the temporal (~2%) and nasal (~2%) areas and in the center (~1.4%) of the retina (Fig. 6A). We did not estimate the proportions of alpha cells in these regions of the neurofilament-stained retina because the densely stained fiber layer prevented reliable counting. Alpha cells were slightly larger in the ventral retina (38 μm, Nissl; 50 μm, neurofilament) compared with other retinal regions (31–35 μm, Nissl; 39–43 μm, neurofilament). The smallest alpha ganglion cell soma sizes were found in the streak/high-density regions (30 μm, Nissl; 35 μm, neurofilament) (Fig. 6B).

ID: jwaa3b2server Time: 21:15 I Path: //chenas03/Cenpro/ApplicationFiles/Journals/Wiley/CNE#/Vol00000/160154/Comp/APPFile/JW-CNE#160154

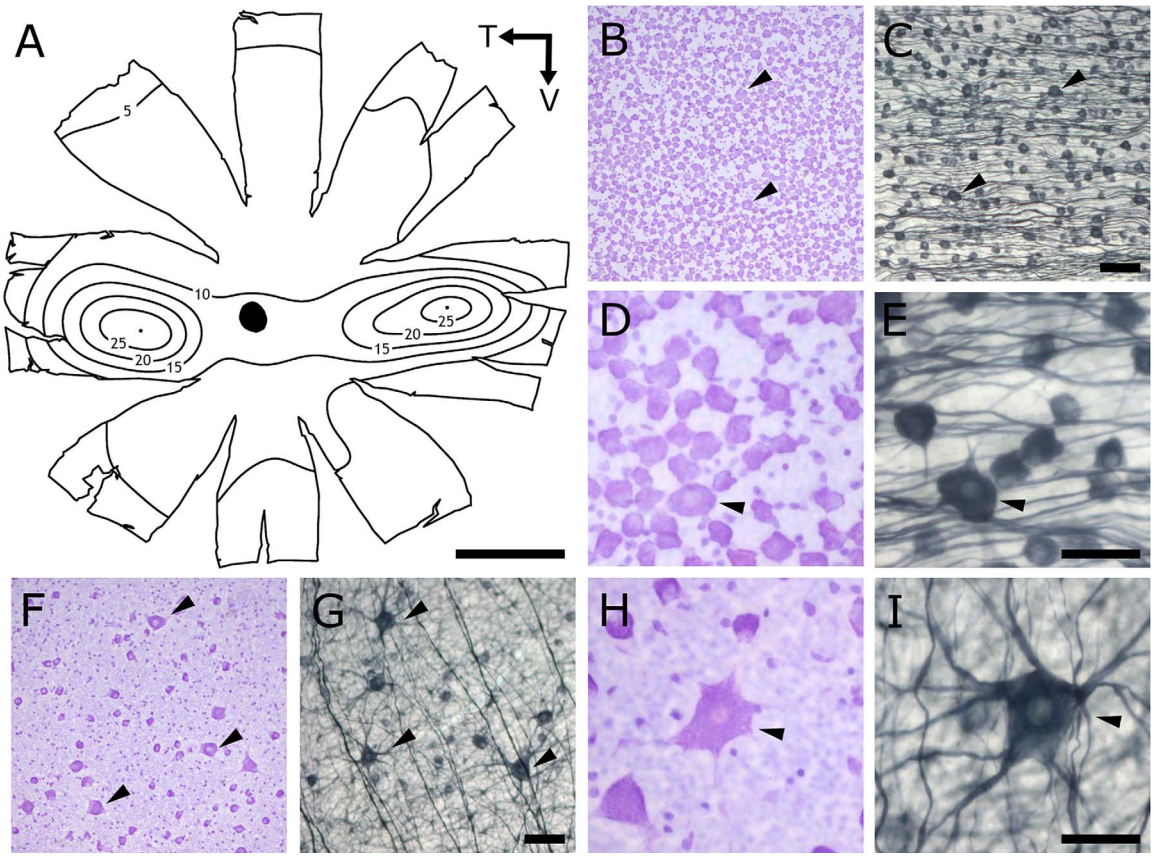

Figure 5. Topographic map illustrating the distribution of alpha retinal ganglion cell densities in the Nissl-stained retinal wholemount of the white rhinoceros (**A**). Note that alpha ganglion cells show a very similar topographic pattern compared with the total ganglion cells. An isodensity line of 5 cells/mm^2 defines a broad and asymmetric plateau, which covers most of the dorsal retina and about half of the ventral retina. Across the nasotemporal axis, an isodensity line of 10 cells/mm^2 demarcate a horizontal streak within which isodensity lines of 15 cells/mm^2 define a temporal and nasal area. Peak densities of alpha cells are marked by dots within the isodensity line of 25 cells/mm^2 in the temporal (44 cells/mm^2) and nasal (40 cells/mm^2) areas. Note that alpha ganglion cells identified in the Nissl-stained retina in regions of high (horizontal streak; **B,D**) and low (ventral; **F,H**) density have a larger soma size and stellate morphology compared with non-alpha cells. Note that similar cytological features are seen in neurofilament-stained alpha cells indicated in equivalent regions of high (horizontal streak; **C,E**) and low (ventral; **G,I**) density. Arrowheads indicate alpha ganglion cell profiles. Numbers on the isodensity lines represent actual densities in cells/mm^2. The black circle in A indicates the position of the optic disc. T, temporal; V, ventral. Scale bars = 10 mm in A; 100 μm in C (also applies to B) and G (also applies to F); 50 μm in E (also applies to D) and I (also applies to H). [Color figure can be viewed at wileyonlinelibrary.com]

Anatomical spatial resolving power

Using an eye axial length of ~29 mm, we estimated a posterior nodal distance of 16.47 mm and a retinal magnification factor of 0.287 mm/deg for the white rhinoceros. Combining these optical estimates with maximum ganglion cell density (~2,000 cells/mm^2, temporal area; ~1,800 cells/mm^2, nasal area), we estimated upper limits of spatial resolving power of 7 cycles/deg for the temporal, and 6.6 cycles/deg for the nasal area. Spatial resolving power in the horizontal streak (maximum ganglion cell density ~800 cells/mm^2) was 4.4 cycles/deg. Based on these estimates of spatial resolving power, we calculated a minimum angle of resolution of ~0.071° for the temporal area, ~0.076° for the nasal area, and ~0.114° for the horizontal streak of the white rhinoceros.

DISCUSSION

In this study, we found that the topographic distribution of retinal ganglion cells in the white rhinoceros reveals an unusual pattern of organization for a terrestrial mammal: a temporal and a nasal area circumscribed by a well-defined horizontal streak. Moreover, we found that the topographic distribution of Nissl-stained alpha ganglion cells reflects a similar dual organization of the total ganglion cell population. We found that the proportions of alpha ganglion cells were higher

ID: jwaa3b2server Time: 21:15 I Path: //chenas03/Cenpro/ApplicationFiles/Journals/Wiley/CNE#/Vol00000/160154/Comp/APPFile/JW-CNE#160154

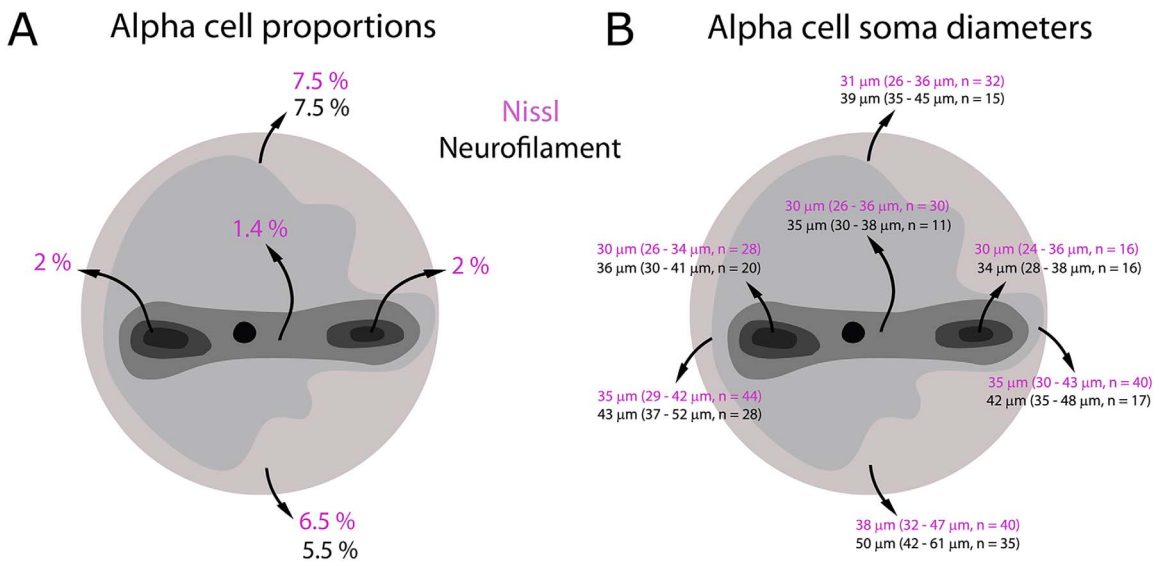

Figure 6. Diagrams illustrating the variation in the proportion (**A**) and soma size (**B**) of Nissl- and neurofilament-stained alpha ganglion cells at different locations of retinal wholemounts of the white rhinoceros. [Color figure can be viewed at wileyonlinelibrary.com]

in the dorsal and ventral portions of the retina. Upper limits of spatial resolving power lie at 7 cycles/deg in the temporal area, 6.6 cycles/deg in the nasal area, and 4.4 cycles/deg in the horizontal streak.

Absence of a tapetum lucidum in the white rhinoceros

The tapetum lucidum is an important specialization that enhances visual sensitivity by reflecting light back to the retina and consequently increasing photon capture in dim light conditions (Duke-Elder, 1958; Land and Nilsson, 2012). Among perissodactyls, a tapetum is found in tapirs and equids (horses, zebras, and asses) but is not found in the greater one-horned rhinoceros (*Rhinoceros unicornis*) (Johnson, 1901). Ophthalmoscopic examination of the eye of the greater one-horned rhinoceros revealed a dull and uniform coloration of the eye fundus suggesting the absence of a tapetum lucidum (Johnson, 1901). Our finding of a homogeneous and dark appearance of the fundus in the white rhinoceros is consistent with the description of the eye fundus of the greater one-horned rhinoceros, supporting the fact that rhinoceroses lack a tapetum lucidum. The adaptive advantage of the absence of a tapetum in the white rhinoceros is unclear because, although this species shows predominant activity when luminance conditions are relatively high, it can also be active during the night for which a tapetum lucidum would be useful (Groves, 1972). A comparison between the numbers and proportions of rod photoreceptors between the rhinoceroses and other perissodactyls would be central to assess whether the rhinoceros eye compensates for the absence of a tapetum lucidum by having a more elevated proportion of rod photoreceptors to improve vision at low light levels.

The dual topographic organization of retinal ganglion cell density

The presence of both a temporal and a nasal area of high ganglion cell density is an uncommon feature in the mammalian retina. This type of arrangement is consistently found in cetaceans (Mass et al., 2013; Mass and Supin, 1986, 1995, 1997; Murayama et al., 1995), but among terrestrial mammals it has only been described for the black rhinoceros (Pettigrew and Manger, 2008). Our finding of a temporal and nasal area of high ganglion cell density in the white rhinoceros is very similar to the topographic pattern described for the black rhinoceros not only in retinal location but also in terms of absolute density. Our estimate of peak ganglion cell density in the temporal area of the white rhinoceros (~2,000 cells/mm^2) is identical to the estimate reported for the black rhinoceros (~2,000 cells/mm^2) (Pettigrew and Manger, 2008). In addition, our estimate of peak density for the nasal area of the white rhinoceros (~1,800 cells/mm^2) is also very similar to, but slightly higher than, the estimate of the black rhinoceros (1,500 cells/mm^2) (Pettigrew and Manger, 2008). Given that the eye sizes of these two species of rhinoceros are very similar (only slightly larger in the white rhinoceros; see below), comparisons of absolute density estimates are reasonable. Even though both studies used a single specimen, the identical results from the two species strongly indicates that a dual

retinal organization is a consistent feature between these two rhinoceros species.

As with the black rhinoceros, our data show that in the white rhinoceros the temporal and nasal areas are embedded within a horizontal streak that extends across the retinal equator. Horizontal streaks are common in species that occur in open environments and facilitate vision across the horizon, presumably by enhancing resolution (Hughes, 1977; Collin, 1999). Because white rhinoceroses occur in open grasslands and savannahs (Groves, 1972; Dinerstein, 2011), the presence of a horizontal streak of high ganglion cell density is compatible with its presumed needs for panoramic vision across the horizon, potentially facilitating the detection of predators and conspecifics. As with most mammals, a temporal area of high retinal ganglion cell density in the white rhinoceros potentially affords increased resolution in the frontal visual field and hence may assist this species to detect physical features of grasses while grazing (Hughes, 1977; Collin, 1999). Although the function of the nasal area is unclear, Pettigrew and Manger (2008) suggested that the nasal area could improve the detection of predators or conspecifics entering the posterior visual field. Here we suggest that the nasal area in the white and black rhinoceroses may have arisen because of their reduced neck mobility and large head size, which hinders head rotations to inspect objects approaching from behind (Leuhold, 2012). Interestingly, the occurrence of a nasal area in the retinas of other mammals that have a limited range of neck mobility (i.e., elephants, cetaceans) gives support to this hypothesis (Pettigrew et al., 2010; Mass et al., 2013; Mass and Supin, 1986, 1995, 1997; Murayama et al., 1995; Leuhold, 2012). Moreover, using ophthalmoscopy, Johnson (1901) indicated that the eye of the rhinoceros shows oblique movements outward and slightly upward, which would facilitate scanning of the posterior visual field by bringing the nasal portion of the retina outward and slightly upward. Therefore, we suggest that a nasal area in the rhinoceroses may represent an important adaptation to compensate for the reduced rotational range of the head and neck and allow for greater sampling of the posterior visual field.

Although the white and black rhinoceros share many similarities in their topographic organization, they differ in the position of the optic disc relative to the horizontal streak, which creates blind spots in different regions of their visual fields. Our results show that in the white rhinoceros the optic disc is located above the horizontal streak, hence creating a blind spot below this specialization in the visual field. This arrangement allows for uninterrupted sampling of the horizon for this species. In contrast, the optic disc in the black rhinoceros is located within the horizontal streak; hence the blind spot interrupts continuous sampling of the horizon (Pettigrew and Manger, 2008). The reasons for these differences are unclear, and it appears paradoxical that the black rhinoceros has a blind spot within one of its high-density specializations. We suggest that, because the black rhinoceros tend to occur in more enclosed vegetation (i.e., woodlands), perhaps sampling of the horizon is not as crucial as for the white rhinoceros, which occurs predominantly in more open microhabitats (Groves, 1972; Hillman-Smith and Groves, 1994). Intriguingly, in the horse—another perissodactyl that occurs in more open microhabitats—the optic disc is located below the horizontal streak (Hebel, 1976; Harman et al., 1999; Guo and Sugita, 2000). This gives support to the idea that the position of the optic disc relative to high-density retinal specializations may be related to specific visual needs to sample environments with different structural complexities.

Topographic specializations of density and proportion of alpha ganglion cells

In mammals, the topographic distribution of alpha ganglion cells generally reflects the pattern of distribution of the total population of retinal ganglion cells (Peichl et al., 1987, Peichl, 1991; Wässle et al., 1975). In the retina of the white rhinoceros, our mapping of alpha ganglion cells revealed a temporal and a nasal area embedded in a horizontal streak, organized in a similar fashion to the distribution of the total population of ganglion cells. Given the role of alpha cells in the detection of brisk transient stimuli and approaching motion (Peichl et al., 1987; Sanes and Masland, 2015), their spatial arrangement in the retina of the white rhinoceros may facilitate panoramic detection of approaching objects (i.e., predators and conspecifics) across the horizon (streak) in addition to the frontal (temporal area) and posterior (nasal area) visual fields. The presence of a nasal area of high density of alpha cells gives further support to the notion that reduced neck flexibility and large body size may have been important evolutionary drivers for the selection of the nasal specializations in the retina of the white rhinoceros. Similar to the white rhinoceros, the giraffe has a high-density area of neurofilament-positive alpha ganglion cells in the dorsonasal retina; however, the density of alpha cells in the giraffe is lower ($\sim$10 cells/mm^2) compared with the white rhinoceros ($\sim$40 cells/mm^2) (Coimbra et al., 2013). In the case of the giraffe, although a nasal peak of alpha cells would still serve the function of facilitating the detection of approaching predators, its lower density probably reflects increased

ID: jwaa3b2server Time: 21:15 I Path: //chenas03/Cenpro/ApplicationFiles/Journals/Wiley/CNE#/Vol00000/160154/Comp/APPFile/JW-CNE#160154

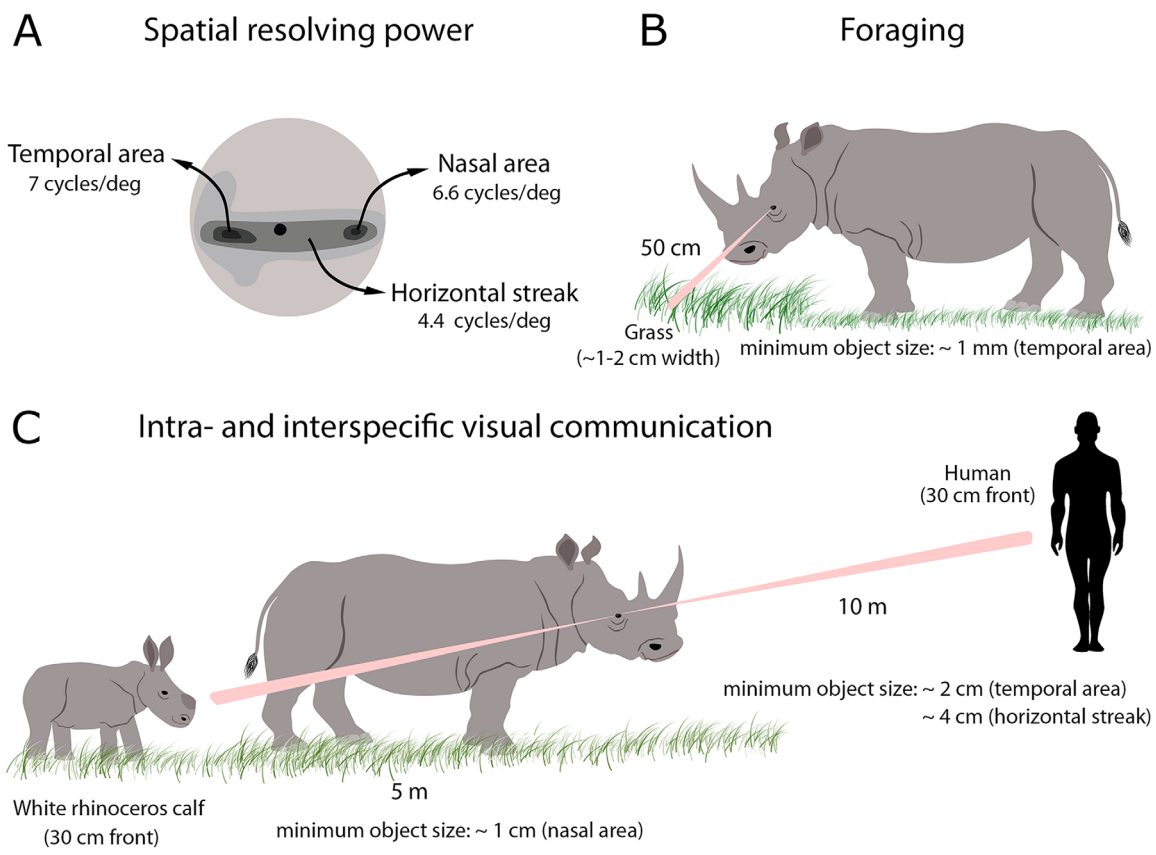

COLOR ONLINE AND BW IN PRINT

Figure 7. Diagram illustrating the levels of spatial resolving power afforded by the topographic retinal specializations of the white rhinoceros (**A**) in the context of foraging (**B**) and detection of conspecifics and predators (**C**). Note the minimum object size potentially resolved by the white rhinoceros at given distances in each scenario. These estimates assume optimum conditions of luminance and contrast. White rhinoceros profile redrawn from Groves and Leslie Jr. (2011). [Color figure can be viewed at wileyonlinelibrary.com]

neck mobility and the ability to rotate its head more freely compared with the white rhinoceros.

In mammals, alpha ganglion cells comprise between 1% and 10% of the total ganglion cell population (Peichl et al., 1987; Peichl, 1991). Our estimate of ~3.5% of alpha ganglion cells is within this range and is very close to the proportion (2–4%) estimated for the cat using Nissl-stained retinas (Wässle et al., 1975). As with other mammals, the proportions of alpha cells in the white rhinoceros vary with retinal location, presumably to enhance detection of approaching objects in portions of the visual field relevant to behavior. Our finding of higher proportions of alpha cells in the dorsal (~7.5%) and ventral (~6.5%) portions of the retina supports this notion. When grazing, the white rhinoceros holds its head at approximately 45° (Groves, 1972), which consequently brings the temporal portion of the retina to view the ground, while the ventral and dorsal portions of the retina sample the front and back of the animal, respectively. The higher proportions of alpha cells in the ventral and dorsal retina would maintain enhanced detection of motion, respectively, in the front and behind the animal, thus compensating for postural adjustments of the head.

Spatial resolving power and visual ecology

Eye size and peak density of retinal ganglion cells represent two key factors that influence the levels of spatial resolving power in mammals (Pettigrew et al., 1998; Veilleux and Kirk, 2014). Our estimates of spatial resolving power for both temporal (7 cycles/deg) and nasal (6.6 cycles/deg) areas in the white rhinoceros are very similar to, although slightly higher than, the estimates reported for the black rhinoceros (temporal, 6 cycles/deg; nasal, 5 cycles/deg) (Pettigrew and Manger, 2008). Because our estimates of peak density of retinal ganglion cells in these specializations are within the same range of the black rhinoceros, these slight differences in spatial resolution are attributable to differences in eye size. The relatively lower spatial resolving power in the black rhinoceros reflects its slightly smaller eye size (axial length, 26.8 mm) (Pettigrew and Manger, 2008) compared with the white rhinoceros (axial length, 29 mm). Interestingly, the relatively similar

ID: jwaa3b2server Time: 21:15 I Path: //chenas03/Cenpro/ApplicationFiles/Journals/Wiley/CNE#/Vol00000/160154/Comp/APPFile/JW-CNE#160154

eye axial lengths of these two species of rhinoceroses suggest that eye size varies little with age given that the black rhinoceros specimen examined by Pettigrew and Manger (2008) was 40 years old, while the white rhinoceros specimen examined in this study was 3 years old. Among other perissodactyls, the higher spatial resolution in the horse (~16.5 cycles/deg) is also a result of larger eye size (axial length, ~38 mm) rather than high ganglion cell density in the temporal area (~5,600 cells/mm^2) (Harman et al., 1999).

Our estimates of spatial resolving power for the white rhinoceros indicate an important role for vision in ecology (Fig. 7). In the context of foraging, with the head held at 50 cm from the ground, the white rhinoceros would be able to resolve a minimum object size of ~1 mm with the spatial resolution afforded by its temporal area (7 cycles/deg). This resolution would be reasonable to detect spatial features of grasses (~1–2 cm) while grazing. At longer distances (~10 m), the spatial resolution of the temporal area and the horizontal streak (4.4 cycles/deg) would afford spatial discrimination of a minimum object size of ~2 cm and ~4 cm, respectively, which would be reasonable to detect a human (~30 cm waistline). At 100 m, resolution of the temporal area would afford discrimination of a minimum object size of 25 cm, which is close to the limits to detect the silhouette of a human. At distances of 5 m, resolution afforded by the nasal area (6.6 cycles/deg) would enable a white rhinoceros to resolve a minimum object size of ~1 cm, which would be reasonable for the discrimination of calves or predators (i.e., hyenas, lions, ~35–40 cm front) approaching the posterior visual field. These estimates assume optimal conditions of contrast and luminance.

CONCLUSIONS

In this study, we show that, similar to the black rhinoceros, the retina of the white rhinoceros exhibits an unusual topographic organization of a temporal and a nasal area embedded within a horizontal visual streak. The functional roles of the temporal area and the horizontal streak are consistent with the white rhinoceros grazing habits and occupation of open environments, respectively. Our finding of a nasal area gives support to a presumed role in the detection of approaching objects in the posterior visual field. We suggest that reduced neck and head mobility of the white rhinoceros may have been an important pressure for selection of the nasal specialization. This is supported by the occurrence of a nasal area in the closely related black rhinoceros, and other species with limited range of head and neck rotations such as cetaceans. The spatial resolution afforded by the areas of retinal specializations is in line with the ecological needs of the white rhinoceros. Moreover, topographic distribution and proportions of alpha ganglion cells also reflect the needs to detect approaching objects across different regions of the visual field. In conclusion, the retina of the white rhinoceros shows a unique set of topographic retinal specializations that indicate an important role for vision in their ecology.

ACKNOWLEDGMENTS

We thank the geographer Luis Barbosa for his immeasurable advice on the use of Arcview software to construct the topographic maps. We thank Malcolm Schuyl for allowing us to use his beautiful white rhinoceros photos.

CONFLICT OF INTEREST STATEMENT

The authors have no conflicts of interest in this study.

ROLE OF AUTHORS

The authors had full access to all the data in the study and take responsibility for the integrity of the data and the accuracy of the data analysis. Study concept and design: JPC, PRM; Collection of specimens: PRM; Collection and acquisition of data: JPC; Analysis and interpretation of the data: JPC, PRM; Writing of the manuscript: JPC; Critical revision of the manuscript for important intellectual content: JPC, PRM; Obtained funding: PRM.

LITERATURE CITED

Coimbra JP, Marceliano MLV, Andrade-da-Costa BLS, Yamada ES. 2006. The retina of tyrant flycatchers: topographic organization of neuronal density and size in the ganglion cell layer of the great kiskadee *Pitangus sulphuratus* and the rusty margined flycatcher *Myiozetetes cayanensis* (Aves: Tyrannidae). Brain Behav Evol 68:15–25.

Coimbra JP, Trévia N, Marceliano MLV, Andrade-da-Costa BLS, Picanço-Diniz CW, Yamada ES. 2009. Number and distribution of neurons in the retinal ganglion cell layer in relation to foraging behaviors of tyrant flycatchers. J Comp Neurol 514:66–73.

Coimbra JP, Nolan PM, Collin SP, Hart NS. 2012. Retinal ganglion cell topography and spatial resolving power in penguins. Brain Behav Evol 80:254–268.

Coimbra JP, Hart NS, Collin SP, Manger PR. 2013. Scene from above: retinal ganglion cell topography and spatial resolving power in the giraffe (*Giraffa camelopardalis*). J Comp Neurol 521:2042–2057.

Coimbra JP, Collin SP, Hart NS. 2014a. Topographic specializations in the retinal ganglion cell layer correlate with lateralized visual behavior, ecology, and evolution in cockatoos. J Comp Neurol 522:3363–3385.

Coimbra JP, Collin SP, Hart NS. 2014b. Topographic specializations in the retinal ganglion cell layer of Australian passerines. J Comp Neurol 522:3609–3628.

Coimbra JP, Kaswera-Kyamakya C, Gilissen E, Manger PR, Collin SP. 2015. The retina of Ansorge's cusimanse (*Crossarchus ansorgei*): number, topography and convergence of photoreceptors and ganglion cells in relation to ecology and behavior. Brain Behav Evol 86:79–93.

Coimbra JP, Kaswera-Kyamakya C, Gilissen E, Manger PR, Collin SP. 2016. The topographic organization of retinal ganglion cell density and spatial resolving power in an unusual arboreal and slow-moving strepsirhine primate, the potto (*Perodicticus potto*). Brain Behav Evol 87:4–18.

Coimbra JP, Pettigrew JD, Kaswera-Kyamakya C, Gilissen E, Collin SP, Manger PR. 2017. Retinal ganglion cell topography and spatial resolving power in African megachiropterans: influence of roosting microhabitat and foraging. J Comp Neurol 525:186–203.

Collin SP. 1999. Behavioural ecology and retinal cell topography. In: Archer SN, Djamgoz, MB, Loew E, Partridge JC, Vallerga S, editors. Adaptive mechanisms in the ecology of vision. London: Chapman & Hall. p 509–535.

de Busserolles F, Marshall NJ, Collin SP. 2014. Retinal ganglion cell distribution and spatial resolving power in deep-sea lanternfishes (Myctophidae). Brain Behav Evol 84:262–276.

Dinerstein E. 2011. Family Rhinocerontidae. In: Wilson DE, Mittermeier RA, editors. Handbook of mammals of the world, vol. 2, Hoofed mammals. Barcelona, Spain: Lynx Edicions. p 144–181.

Dräger UC, Hofbauer A. 1984. Antibodies to heavy neurofilament subunit detect a subpopulation of damaged ganglion cells in retina. Nature 309:624–626.

Duke-Elder S. 1958. The eye of mammals. In: System of Ophthalmology, vol 1, The eye in evolution. London: Henry Kimpton. p 495–496.

Glaser EM, Wilson PD. 1998. The coefficient of error of optical fractionator population size estimates: a computer simulation comparing three estimators. J Microsc 192: 163–171.

Groves CP. 1972. *Ceratotherium simum*. Mammalian species 8:1–6.

Gundersen HJG. 1977. Notes on the estimation of the numerical density of arbitrary profiles: the edge effect. J Microsc 111:219–223.

Gundersen HJG, Bagger P, Bendtsen TF, Evans SM, Korbo L, Marcussen N, Møller A, Nielsen K, Nyengaard JR, Pakkenberg B, Sørensen FB, Vesterby A, West MJ. 1988. The new stereological tools: disector, fractionator, nucleator and point sampled intercepts and their use in pathological research and diagnosis. APMIS 96:857–881.

Guo X, Sugita S. 2000. Topography of ganglion cells in the retina of the horse. J Vet Med Sci 62:1145–1150.

Harman AM, Moore S, Hoskins R, Keller P. 1999. Horse vision and an explanation for the visual behaviour originally explained by the 'ramp retina'. Equine Vet J 5:384–390.

Hebel R. 1976. Distribution of retinal ganglion cells in five mammalian species (pig, sheep, ox, horse, dog). Anat Embryol 150:45–51.

Hillman-Smith AKK, Groves CP. 1994. *Diceros bicornis*. Mammalian Species 455:1–8.

Hubert T, Bourane S, Venteo S, Mechaly I, Puech S, Valmier J, Carroll P, Fichard-Carroll A. 2008. Fibroblast growth factor homologous factor 1 (FHF1) is expressed in a subpopulation of calcitonin gene-related peptide-positive nociceptive neurons in the murine dorsal root ganglia. J Comp Neurol 507:1588–1601.

Hughes A. 1977. The topography of vision in mammals of contrasting life style: comparative optics and retinal organisation. In: Crescitelli F, editor. Handbook of sensory physiology, vol. VII/5: The visual system of vertebrates. Berlin: Springer Verlag. p 613–756.

Hughes A. 1981a. Population magnitudes and distribution of the major modal classes of cat retinal ganglion cell as estimated from HRP filling and a systematic survey of the soma diameter spectra for classical neurones. J Comp Neurol 197:303–339.

Hughes A. 1981b. Cat retina and the sampling theorem; the relation of transient and sustained brisk-unit cut–off frequency to alpha and beta-mode cell density. Exp Brain Res 42:196–202.

Johnson GL. 1901. Contributions to the comparative anatomy of the mammalian eye, chiefly based on ophthalmoscopic examination. Philos Trans R Soc Lond B 194:1–82.

Land MF, Nilsson D-E. 2012. Animal eyes. New York:Oxford University Press.

Leuhold W. 2012. African ungulates: a comparative approach of their ethology and behavioral ecology. New York: Springer Science and Business Media.

Lisney TJ, Iwaniuk AN, Kolominsky J, Bandet MV, Corfield JR, Wylie DR. 2012. Interspecifc variation in eye shape and retinal topography in seven species of galliform bird (Aves: Galliformes: Phasianidae). J Comp Physiol A 198: 717–731.

Lisney TJ, Stecyk K, Kolominsky J, Schmidt BK, Corfield JR, Iwaniuk AN, Wylie DR. 2013a. Ecomorphology of eye shape and retinal topography in waterfowl (Aves: Anseriformes: Anatidae) with different foraging modes. J Comp Physiol A 199: 385–402.

Lisney TJ, Stecyk K, Kolominsky J, Graves GR, Wylie DR, Iwaniuk AN. 2013b. Comparison of eye morphology and retinal topography in two species of new world vultures (Aves: Cathartidae). Anat Rec 296:1954–1970.

Manger PR, Pillay P, Maseko BC, Bhagwandin A, Gravett N, Moon DJ, Jillani N, Hemingway J. 2009. Acquisition of brains from the African elephant (*Loxodonta africana*): Perfusion-fixation and dissection. J Neurosci Methods 179:16–21.

Mass AM, Supin AY. 1986. Topographic distribution of sizes and density of ganglion cells in the retina of a porpoise, *Phocoena phocoena*. Aquat Mammal 12:95–102.

Mass AM, Supin AY. 1992. Peak density, size and regional distribution of ganglion cells in the retina of the fur seal *Callorhinus ursinus*. Brain Behav Evol 39:69–76.

Mass AM, Supin AY. 1995. Ganglion cells topography of the retina in the bottlenosed dolphin, *Tursiops truncatus*. Brain Behav Evol 45:257–265.

Mass AM, Supin AYa. 1997. Ocular anatomy, retinal ganglion cell distribution, and visual resolution in the gray whale, *Eschrichtius gibbosus*. Aquat Mammal 23:17–28.

Mass AM, Supin AY, Abramov AV, Mukhametov LM, Rozanova EI. 2013. Ocular anatomy, ganglion cell distribution and retinal resolution of a killer whale (*Orcinus orca*). Brain Behav Evol 81:1–11.

Moraes AMM, Oliveira MMM, Hokoc JN. 2000. Retinal ganglion cells in the South American opossum (*Didelphis aurita*). J Comp Neurol 418:193–216.

Murayama T, Somiya H, Aoki I, Ishii T. 1995. Retinal ganglion cell size and distribution predict visual capabilities of Dall's porpoise. Mar Mammal Sci 11:136–149.

Peichl L. 1991. Alpha ganglion cells in mammalian retinae: common properties, species differences, and some comments on other ganglion cells. Vis Neurosci 7:155–169.

Peichl L. 1992. Topography of ganglion cells in the dog and wolf retina. J Comp Neurol 324:603–620.

Peichl L, Ott H, Boycott BB. 1987. Alpha ganglion cells in mammalian retinae. Proc R Soc Lond B Biol Sci 231:169–197.

Pettigrew JD, Manger PR. 2008. Retinal ganglion cell density of the black rhinoceros (*Diceros bicornis*): calculating visual resolution. Vis Neurosci 25:215–220.

Pettigrew JD, Dreher B, Hopkins CS, McCall MJ, Brown M. 1988. Peak density and distribution of ganglion cells in the retinae of microchiropteran bats: implications for visual acuity. Brain Behav Evol 32:39–56.

Pettigrew JD, Bhagwandin A, Haagensen M, Manger PR. 2010. Visual acuity and heterogeneities of retinal ganglion cell densities and the tapetum lucidum of the African elephant (*Loxodonta africana*). Brain Behav Evol 75:251–261.

Price SA, Bininda-Emonds ORP. 2009. A comprehensive phylogeny of extant horses, rhinos and tapirs (Perissodactyla) through data combination. Zoosyst Evol 85:277–292.

Reuter T, Peichl L. 2008. Structure and function of the retina in aquatic tetrapods. In: Thewissen JGM, Nummela S, editors. Sensory evolution on the threshold—adaptations in secondarily aquatic vertebrates. Berkeley, CA: University of California Press. p 149–172.

Ruiz-Ederra J, García M, Hicks D, Vecino E. 2004. Comparative study of the three neurofilament subunits within pig and human retinal ganglion cells. Mol Vis 10:83–92.

Sanes JR, Masland RH. 2015. The types of retinal ganglion cells: current status and implications for neuronal classification. Annu Rev Neurosci 38:221–246.

Saper CB, Sawchenko PE. 2003. Magic peptides, magic antibodies: guidelines for appropriate controls for immunohistochemistry. J Comp Neurol 465:161–163.

Silveira LCL, Picanço-Diniz CW, Sampaio L, Oswaldo-Cruz E. 1989a. Retinal ganglion cell distribution in the cebus monkey: a comparison with the cortical magnification factors. Vision Res 29:1471–1483.

Silveira LCL, Picanço-Diniz CW, Oswaldo-Cruz E. 1989b. Distribution and size of ganglion cells in the retinae of large Amazon rodents. Vis Neurosci 2:221–235.

Slomianka L, West MJ. 2005. Estimators of the precision of stereological estimates: an example based on the CA1 pyramidal cell layer of rats. Neuroscience 136:757–767.

Snyder AW, Miller WH. 1977. Photoreceptor diameter and spacing for highest resolving power. JOSA 67:696–698.

Stone J. 1981. The wholemount handbook: a guide to the preparation and analysis of retinal wholemounts. Sydney, Australia:Maitland Publications.

Straznicky C, Vickers JC, Gábriel R, Costa M. 1992. A neurofilament protein antibody selectively labels a large ganglion cell type in the human retina. Brain Res 582:123–128.

Veilleux CC, Kirk EC. 2014. Visual acuity in mammals: effects of eye size and ecology. Brain Behav Evol 83:43–53.

Wässle H. 2004. Parallel processing in the mammalian retina. Nat Rev Neurosci 5:747–757.

Wässle H, Levick WR, Cleland BG. 1975. The distribution of the alpha type of ganglion cells in the cat's retina. J Comp Neurol 159:419–438.

West MJ, Slomianka L, Gundersen HJG. 1991. Unbiased stereological estimation of the total number of neurons in the subdivisions of the rat hippocampus using the optical fractionator. Anat Rec 231:482–497.

Williams DR, Coletta NJ. 1987. Cone spacing and the visual resolution limit. JOSA A 4:1514–1523.

Wong ROL, Wye-Dvorak J, Henry GH. 1986. Morphology and distribution of neurons in the retinal ganglion cell layer of the adult tammar wallaby - *Macropus eugenii*. J Comp Neurol 253:1–12.

Yamanaka H, Kobayashi K, Okubo M, Fukuoka T, Noguchi K. 2011. Increase of close homolog of cell adhesion molecule L1 in primary afferent by nerve injury and the contribution to neuropathic pain. J Comp Neurol 519:1597–1615.

SGML and CITI Use Only
DO NOT PRINT

The white rhinoceros retina shows an unusual topographic organization of high ganglion cell density formed by a temporal and a nasal area embedded in a horizontal streak. The nasal area may enhance visual sampling of the posterior visual field compensating for the reduced neck mobility in this species.